Geothermics 51 (2014) 312–324

Contents lists available at ScienceDirect

Geothermics

journal homepage: www.elsevier.com/locate/geothermics

# 3D numerical modeling of vertical geothermal heat exchangers

T.Y. Ozudogru [a,b,*], C.G. Olgun [b], A. Senol [a]

[a] Department of Civil Engineering, Istanbul Technical University, 34469 Maslak, Istanbul, Turkey
[b] Charles E. Via, Jr. Department of Civil and Environmental Engineering, Virginia Tech, Blacksburg, VA 24061, USA

ARTICLE INFO

*Article history:*
Received 14 June 2013
Accepted 17 February 2014
Available online 15 March 2014

*Keywords:*
Borehole heat exchanger
Energy pile
3D numerical model
Model validation
Finite line source

ABSTRACT

This paper presents the development and validation of a 3D numerical model for simulating vertical U-tube geothermal heat exchangers (GHEs). For minimizing the computational effort, the proposed numerical model uses 1D linear elements for simulating the flow and heat transfer inside the pipes. These linear elements are coupled with the 3D domain using the temperature field along the exterior surface of the pipe and an optimized finite element mesh for reducing the number of elements. The discretization of geometry, finite element mesh generation and the specifics of the system physics and boundary condition assignments are explained in detail. The model is used to simulate two generic cases, a borehole with a single U-tube and an energy pile with double U-tubes. In each case, a constant heating followed by a recovery period (i.e., no heating) is simulated. A review of the theory of finite line source model is also presented, along with modifications to account for variable heat rate. Moreover, a method to estimate the steady state thermal resistances in the borehole/energy pile is presented in order to calculate the fluid temperatures analytically. The validation of the model is carried out by comparing the numerical results with the results obtained from the analytical model.



## 1. Introduction and background

Geothermal heat pump (GHP) or ground-coupled heat pump (GCHP) systems are a promising and highly efficient renewable energy technology for space heating and cooling (Sanner et al., 2003; Lund et al., 2011). They are recognized by the Energy Star Joint Program as being among the most efficient and comfortable heating and cooling systems because they use the ground as a natural heat source and sink (Energy Star, 2013). Over the past 15 years, the technology has shown annual increases of 16.6% worldwide, with number of installed units at 2.76 million (Lund et al., 2011), which illustrates the high acceptance of this emerging technology in the heating, ventilation, and air conditioning (HVAC) market. By comparison with the conventional technologies, these heat pumps offer better levels of comfort, reduced noise levels, lower greenhouse gas emissions and reasonable environmental safety (Bandos et al., 2011). Electrical consumption and maintenance requirements of GCHP systems are lower than those required by conventional systems and consequently these systems have lower annual operating costs (Yu et al., 2002).

This technology relies on the fact that, after a depth of 5 to 10 m, the ground has a relatively constant temperature, warmer than the ambient temperature in the winter and cooler in the summer. A geothermal heat pump can transfer the heat stored in the ground into a building during the winter, and collect the heat from the building and inject it into the ground during the summer (Omer, 2008). Therefore, the efficiency of GCHP systems is inherently higher than that of air-source heat pumps because the average ground temperature serves a better baseline for heating and cooling in the winter and summer, respectively.

GCHP systems consist of a sealed loop of pipes, buried in the ground and connected to a heat pump (Bose, 1991). They use the ground as a heat source when operating in heating mode, with a fluid (usually water or a water–antifreeze mixture) as the medium that transfers the heat from the ground to the evaporator of the heat pump, thus utilizing near-surface geothermal energy. In cooling mode, they use the ground as a heat sink (Sanner et al., 2003). A vertical borehole configuration is usually preferred over horizontal trench systems because it requires less foot print and vertical systems bypass the shallow zone influenced by ambient temperatures and utilize the constant temperature of the ground. In vertical borehole systems, the geothermal heat exchanger (GHE) consists of a number of boreholes or energy piles, each containing several U-tubes. Energy piles are a relatively new ground-coupled heat exchanger technology in which the circulation pipes are

* Corresponding author at: Department of Civil Engineering, Istanbul Technical University, 34469 Maslak, Istanbul, Turkey. Tel.: +90 212 285 6628.
*E-mail addresses:* ozudogru@itu.edu.tr, ozudogru@gmail.com (T.Y. Ozudogru).

http://dx.doi.org/10.1016/j.geothermics.2014.02.005
0375-6505/

**Nomenclature**

| | |
|---|---|
| $A$ | cross-section area ($m^2$). |
| $C_A$, $C_B$ | factors in Eq. (16) |
| $c_p$ | specific heat capacity ($J\,kg^{-1}\,K^{-1}$) |
| $d$ | diameter (m) |
| $d_h$ | hydraulic diameter of pipe (m) |
| Ei($x$) | exponential integral |
| $f_D$ | Darcy friction factor |
| $h$ | overall heat transfer coefficient ($W\,m^{-2}\,K^{-1}$) |
| $H$ | length of the heat exchanger (m) |
| $k$ | thermal conductivity ($W\,m^{-1}\,K^{-1}$) |
| Nu | Nusselt number |
| $p$ | pressure (Pa) |
| $q_{wall}$ | external heat exchange through pipe wall (W) |
| $q$ | heat (W) |
| $q'$ | heat flux per unit depth ($W\,m^{-1}$) |
| $q''$ | heat flux per unit area ($W\,m^{-2}$) |
| $r$ | radius (m) |
| $R$ | thermal resistance ($m\,K\,W^{-1}$) |
| Re | Reynolds number |
| $T$ | temperature (K) |
| $t$ | time (s) |
| $t_s$ | time scale (s) |
| $\dot{V}$ | volumetric flow rate ($m^3\,s^{-1}$) |
| $\mathbf{u}$ | velocity field ($m\,s^{-1}$) |
| $Z$ | wetted perimeter of pipe (m) |

*Greek symbols*

| | |
|---|---|
| $\alpha$ | thermal diffusivity ($m^2\,s^{-1}$) |
| $\Delta T(t)$ | applied temperature difference at time $t$ (K) |
| $\zeta$ | distance between the actual point heat source and the point of interest (m) |
| $\zeta'$ | distance between the imaginary point heat source and the point of interest (m) |
| $\mu$ | dynamic viscosity (Pa s) |
| $\rho$ | density ($kg\,m^{-3}$) |

*Subscripts*

| | |
|---|---|
| b | borehole/pile |
| bw | borehole/pile wall |
| eff | effective |
| ext | external |
| f | fluid |
| g | ground |
| i | inside |
| in | inlet |
| int | internal |
| o | outside |
| out | outlet |
| p | pipe |

integrated into a pile foundation that provides structural support for the building (Brandl, 2006). With vertical geothermal heat exchangers, geothermal heat pumps can offer both heating and cooling at virtually any location, with great flexibility to meet the energy demands (Sanner et al., 2003).

Over the years, various analytical and numerical models of varying complexities have been developed and used as a design tool for GHEs. Among other things, they can be used to predict temperatures in and around the GHE utilizing the heat transfer mechanisms inside a borehole, the conductive heat transfer from a borehole and the thermal interferences between boreholes. A number of design tools based on flnite element or flnite volume programs were used to develop fully discretized borehole heat exchanger models to include transient effects, as well as the correct borehole geometry. Some of the most noteworthy models include the studies by Al-Khoury et al. (2005), Al-Khoury and Brinkgreve (2006), Signorelli et al. (2007), Marcotte and Pasquier (2008), Lamarche et al. (2010) and He (2012). Some of the models were limited to 2D discretization because of the number of small elements needed for a sufficient discretization of the borehole cross section (Austin, 1998; Yavuzturk, 1999). On the other hand, several hybrid models were developed to provide a feasible alternative (Eskilson, 1987; Yavuzturk and Spitler, 1999). Such models are used to calculate the temperature response functions numerically. Analytical models, despite being less precise than numerical models, are preferred in most practical applications because of their superior computation time efficiencies and better flexibility for parametric design. The inaccuracy in the results of the analytical models corresponds to the underlying modeling assumptions made when deriving analytical solutions for GHEs. However, it must be kept in mind that uncertainties regarding the quality of input data may be more significant than uncertainties due to modeling approximations.

On the contrary, if a correct description of the geometry and heat transfer mechanisms inside and outside the GHE is needed, 3D numerical models must be used. Only 3D models can capture the vertical heat transfer inside and outside the GHE. They can be utilized to model layered ground profiles, the vertical gradient of the undisturbed ground temperature, the flow and transient heat transfer of the fluid inside the tubes, the thermal short-circuiting between the tube legs, and also they allow assigning proper boundary conditions at the upper and lower model boundaries. The main disadvantage of fully discretized 3D models is their extensive computation time, even with the help of modern and powerful computers and the possibility of parallel computing. For instance, a single simulation of an ordinary borehole thermal conductivity test takes from a few hours to several days. As a consequence, the application of fully discretized models for automated parameter estimation procedures with various iterations becomes impractical (Bauer et al., 2011).

In this study, we have developed a numerical modeling approach to overcome these problems. We utilized a commercially available finite elements simulation environment, COMSOL Multiphysics™ (COMSOL, 2012) and developed a numerical model for vertical GHEs that can calculate the 3D transient heat and mass transport processes in the borehole and/or energy pile with satisfactory accuracy and minimal computational effort. This approach can be applied to automated parameter estimation procedures for thermal conductivity data evaluation. The proposed numerical model distinctively uses 1D linear elements for simulating the flow and heat transfer inside the pipes, which is fully coupled with the 3D geometry using the temperature field at the pipe exterior surface. In the recent studies by Corradi et al. (2008) and Zanchini et al. (2010a, 2010b), the distribution of the fluid bulk temperature along the flow direction and the heat transfer between the fluid and the pipe wall are evaluated by making use of weak form boundary condition available in COMSOL Multiphysics™.

The model utilizes swept finite element meshing in the vertical direction, and the mesh is optimized to minimize the number of elements. However, the reduction should not be done at the expense of obtaining numerical results with poor accuracy. Prior experience shows that, mesh refinement is required near the ground surface, soil/rock layer interfaces and the toe of the heat exchanger, where larger vertical temperature gradients reside. Minimum refinement is necessary in mid-layers, where vertical temperature gradients are negligible. A similar meshing technique was used in a study by Marcotte and Pasquier (2008).

This paper details the development of the proposed 3D numerical model, explaining the theory governing the thermal processes, finite element mesh generation and selection of the appropriate boundary conditions. The numerical model is used to simulate two generic cases, a borehole with a single U-tube and an energy pile with double U-tubes, respectively. In each case, a constant heating followed by a recovery period (i.e., no heating) is simulated. A review of the theory of finite line source model is also presented, along with modifications for variable heat rate. Moreover, a method to estimate the thermal resistances in the borehole/energy pile is introduced in order to calculate the fluid temperatures analytically. The validation of the model is carried out by comparing the numerical results with the results obtained from the analytical model.

## 2. Finite line source model

Finite line source model (FLS) is a special case of the line source model, which is a direct application of Lord Kelvin's point heat source approach to ground coupled heat exchangers (Thomson, 1884). It relies on the principle of superposition where a line consists of a combination of sequentially positioned points. Thus, it starts with calculating the temperature change at specific location in an infinite homogeneous medium based on the formula of point heat source, then integrating along a line to account for the effect of point sources positioned along the line. The model is called infinite line source (ILS) model when the integral of the point source formula is performed on a line with an infinite length. When a line source with a finite length is considered, the model is called finite line source model, which is used to account for the end effects of the GHE.

Ingersoll and Plass (1948) showed that the temperature change at time $t$ and at a distance $\zeta$ from a point heat source emitting constant heat of $q$ can be calculated as follows:

$$\Delta T(t) = \left(\frac{q\alpha}{k}\right)\left(\frac{1}{2\sqrt{\pi\alpha t}}\right)^3 \exp\left(-\frac{\zeta^2}{4\alpha t}\right) \tag{1}$$

Integrating Eq. (1) over the distance extending from negative infinity to positive infinity, the expression for the ILS model is obtained as:

$$\Delta T(t) = \frac{q}{4\pi k}\mathrm{Ei}\left(-\frac{r^2}{4\alpha t}\right) \tag{2}$$

Zeng et al. (2002) developed an approach to estimate the temperature changes in a homogenous semi-infinite medium induced by a finite line source. The model accounts for the end effects of the GHE by including a virtual line sink with the same length as the GHE but with a negative heating rate $-q$ on symmetry to the ground surface boundary (Fig. 1). This ensures that the temperature at the ground surface is kept constant throughout the period considered.

The FLS model can be derived by integrating Eq. (1) over the length of the heat exchanger and including the identical yet opposite imaginary source. The final form of the FLS model equation is given as:

$$\Delta T(t) = \left(\frac{q}{4\pi k}\right)\int_0^H \left[\frac{\mathrm{erfc}(\sqrt{r^2+(z-h)^2}/2\sqrt{\alpha t})}{\sqrt{r^2+(z-h)^2}} - \frac{\mathrm{erfc}(\sqrt{r^2+(z+h)^2}/2\sqrt{\alpha t})}{\sqrt{r^2+(z+h)^2}}\right] \mathrm{dh} \tag{3}$$

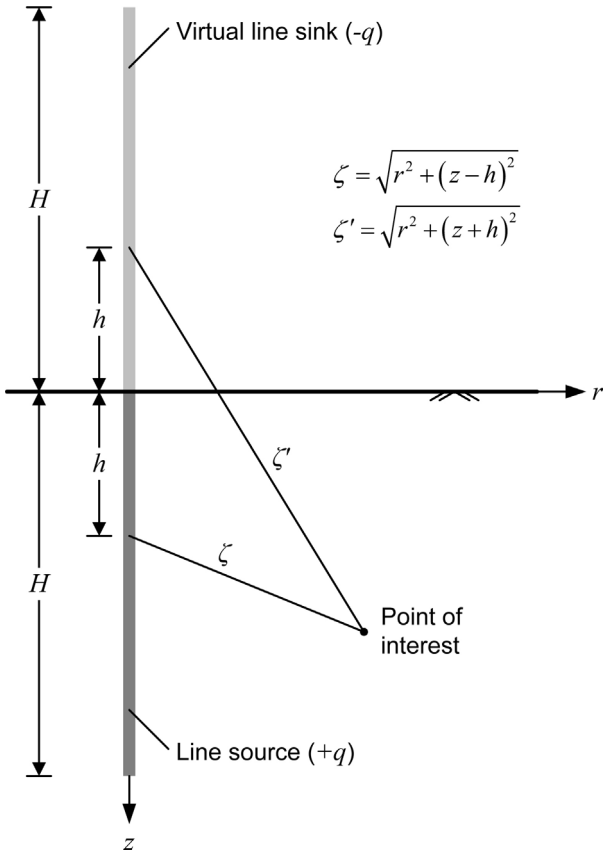


**Fig. 1.** The geometry of the finite line source model (after Zeng et al., 2002).

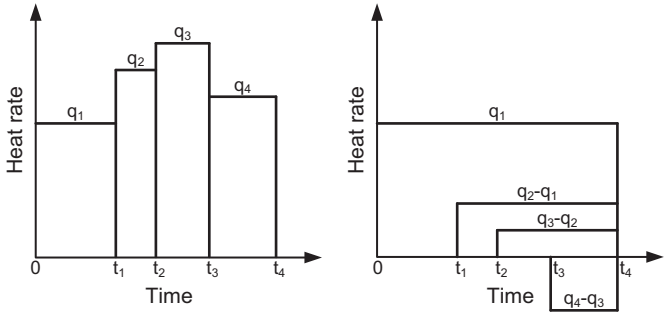


**Fig. 2.** The superposition principle for varying heat rate (after Yang et al., 2009).

## 3. Variable heat rate

The infinite line source and the finite line source models rely on the assumption of constant heat rate throughout the heating or cooling period. The analytical model needs to be modified to consider varying heat rate, such as the recovery period after applying a heat load for a certain period of time. Yang et al. (2009) proposed a method to account for the varying heat rate in ILS, which uses step loading and utilizes the principle of superposition in the time domain. In this approach the ILS expression for the varying heat rate given in Fig. 2 is defined as:

$$\Delta T(t) = \frac{q_1}{4\pi k}\mathrm{Ei}\left(-\frac{r^2}{4\alpha t_4}\right) + \frac{q_2-q_1}{4\pi k}\mathrm{Ei}\left[-\frac{r^2}{4\alpha(t_4-t_1)}\right] + \frac{q_3-q_2}{4\pi k}\mathrm{Ei}\left[-\frac{r^2}{4\alpha(t_4-t_2)}\right] + \frac{q_4-q_3}{4\pi k}\mathrm{Ei}\left[-\frac{r^2}{4\alpha(t_4-t_3)}\right] \tag{4}$$

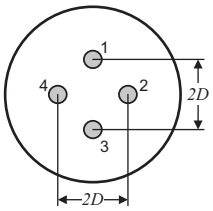


**Fig. 3.** Cross-section of a double U-tube borehole (after Zeng et al., 2003).

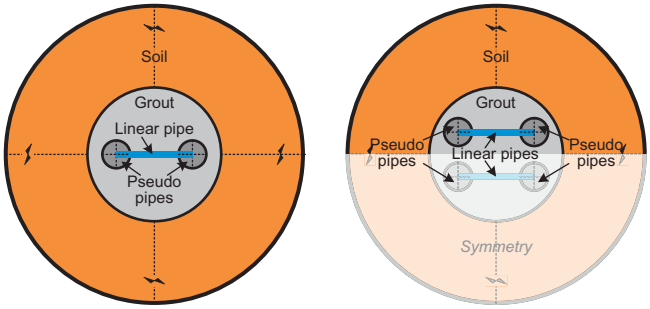


**Fig. 4.** Cross-sections and elements of single and double loop models.

Using the same principle, to account for the varying heat rate for a heating period of $t_1$ and afterwards a recovery period of $(t_2 - t_1)$, Eq. (3) for FLS is modified as follows:

$$\Delta T(t) = \left(\frac{q}{4\pi k}\right) \int_0^H \left[ \frac{\operatorname{erfc}\left(\sqrt{r^2+(z-h)^2}/2\sqrt{\alpha t_2}\right) - \operatorname{erfc}\left(\sqrt{r^2+(z-h)^2}/2\sqrt{\alpha (t_2-t_1)}\right)}{\sqrt{r^2+(z-h)^2}} - \frac{\operatorname{erfc}\left(\sqrt{r^2+(z+h)^2}/2\sqrt{\alpha t_2}\right) - \operatorname{erfc}\left(\sqrt{r^2+(z+h)^2}/2\sqrt{\alpha (t_2-t_1)}\right)}{\sqrt{r^2+(z+h)^2}} \right] \mathrm{dh} \tag{5}$$

## 4. Borehole thermal resistance

The analytical models such as the finite line source can be used to calculate the temperature changes in the ground, starting from the borehole/pile wall. In order to estimate the mean fluid temperature inside the tubes, borehole thermal resistance must be known. The relationship between the mean fluid temperature and the borehole wall temperature is given as:

$$T_f = T_{bw} + \frac{q}{H} R_b \tag{6}$$

Many factors have impact on the borehole resistance, including the diameter of the borehole, the thermal conductivity and the diameters of the U-tubes, their shank spacing, thermal conductivities of the backfill and the ground, flow rate of the fluid and its thermal properties, as well as the flow circuit arrangement. The borehole resistance is a transient parameter, as it starts from zero and approaches a constant value, which is called the steady state borehole resistance. It is common practice that the heat transfer inside the borehole is approximated as a steady-state process, as the temperature variation inside the borehole is usually slow and minor. Such simplification has been proved appropriate and convenient for most engineering practices except for the analysis dealing with dynamic responses considering time scales of a few hours (Yavuzturk, 1999).

Different methods to estimate the steady state borehole resistance have been proposed by various researchers and these include equivalent diameter expression (Gu and O'Neal, 1998), shape factors (Paul, 1996), multipole expansions approach (Bennet et al., 1987), line source approximation (Hellström, 1991). In this study, we have used Hellström's line source approach as presented by Zeng et al. (2003) because in addition to its simplicity, it provides results with reasonable accuracy and can be extended to double loop configurations.

For the borehole with double U-tube configuration given in Fig. 3, the difference between fluid temperatures in each pipe and the borehole wall can be expressed in terms of heat fluxes per unit length in each pipe and a set of thermal resistances:

$$\begin{aligned} T_{f1} - T_{bw} &= R_{11}q_1 + R_{12}q_2 + R_{13}q_3 + R_{14}q_4 \\ T_{f2} - T_{bw} &= R_{21}q_1 + R_{22}q_2 + R_{23}q_3 + R_{24}q_4 \\ T_{f3} - T_{bw} &= R_{31}q_1 + R_{32}q_2 + R_{33}q_3 + R_{34}q_4 \\ T_{f4} - T_{bw} &= R_{41}q_1 + R_{42}q_2 + R_{43}q_3 + R_{44}q_4 \end{aligned} \tag{7}$$

In Eq. (7), $R_{ii}$ denotes the thermal resistance between the circulating fluid in a certain U-tube leg and the borehole wall, and $R_{ij}$ is the thermal resistance between two individual pipes. The solution of Hellström's line source assumption is expressed as:

$$\begin{aligned} R_{11} &= \frac{1}{2\pi k_b}\left[\ln\left(\frac{r_b}{r_{po}}\right) - \frac{k_b - k_g}{k_b + k_g}\ln\left(\frac{{r_b}^2 - D^2}{r_b^2}\right)\right] + R_p \\ R_{12} &= \frac{1}{2\pi k_b}\left[\ln\left(\frac{r_b}{\sqrt{2}D}\right) - \frac{k_b - k_g}{2\left(k_b + k_g\right)}\ln\left(\frac{r_b^4 + D^4}{r_b^4}\right)\right] \\ R_{13} &= \frac{1}{2\pi k_b}\left[\ln\left(\frac{r_b}{2D}\right) - \frac{k_b - k_g}{k_b + k_g}\ln\left(\frac{r_b^2 + D^2}{r_b^2}\right)\right] \end{aligned} \tag{8}$$

The pipe resistance $R_p$ is a combination of the convective resistance of the fluid and the conduction resistance of the pipe wall. It is defined by the expression:

$$R_p = \frac{1}{2\pi r_{pi} h_{int}} + \frac{\ln(r_{po}/r_{pi})}{2\pi k_p} \tag{9}$$

Finally, the overall resistance of the GHE is evaluated as an average of thermal resistances between individual pipes:

$$R_b = \frac{R_{11} + R_{12} + R_{23} + R_{13}}{4} \tag{10}$$

## 5. Model development and finite element mesh

The proposed numerical model of the GHE consists of several components. These include the pipes, the grout/backfill, and the soil/rock surrounding the heat exchanger. The lateral and bottom extents of the model are selected such that no thermal interaction occurs across the external boundaries. The diameter of the pipe elements is taken equal to the pipe outside diameter and these elements are identified as 'pseudo pipes'.

The actual physical representation of the pipes and the circulated fluid is modeled using a line element that crosses between the center-axes of pseudo pipes in each individual loop. On the other hand, pseudo pipes are used to compensate for the temperature coupling error which will be discussed in the following sections. The cross-sections of typical GHE configurations (single loop and double loop) showing the model components are schematically given in Fig. 4. Symmetry could not be used in the discretization

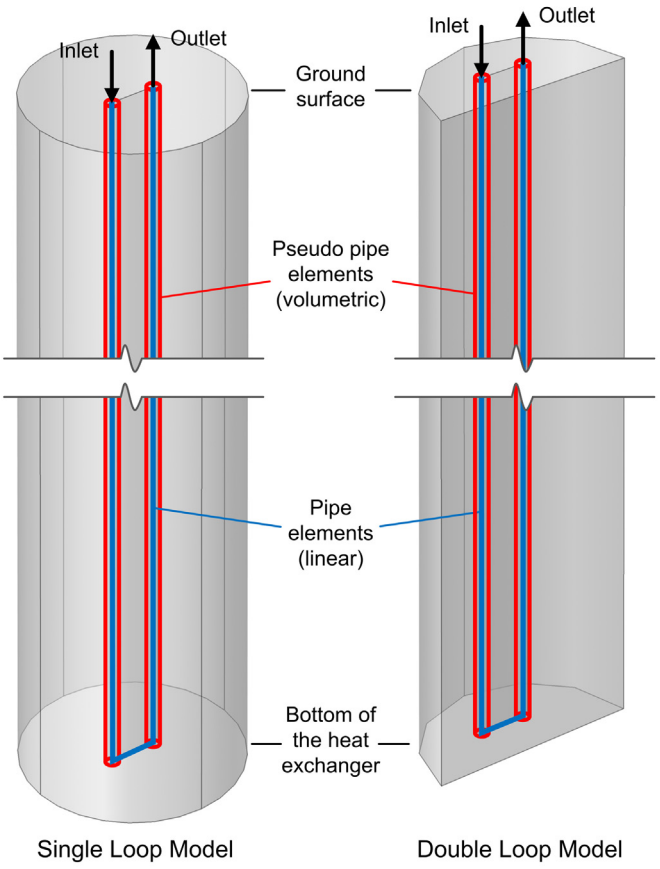


**Fig. 5.** Linear pipe elements and volumetric pseudo pipe elements.

of the single loop model; because the linear pipe element cannot be divided. On the contrary, double loop models can benefit from symmetry if the operation of the GHE is performed in parallel connection, which greatly reduces the computation time.

Two dimensional elements are generated at the ground surface for all the model components and extruded downward. The extrusion is controlled by the toe of the borehole/energy pile, and the boundaries between various soil layers. These controlling locations horizontally divide the 3D domain into soil layers, thus various properties can be assigned for each layer accordingly. With the help of the linear pipe elements, the extrusion of the horizontal plane allows the creation of continuous line elements by establishing a connection between downward and upward pipes at the toe of the GHE. Fig. 5 provides more insight into the linear pipes and the pseudo pipe approach, presenting the 3D extruded geometry.

The finite element mesh of the proposed model is generated in a similar way to the discretization of the geometry. First, the horizontal plane on the ground surface is meshed using triangular elements, and then the generated mesh on this plane is swept downward until the limits of the model, to obtain the overall finite element mesh which consists of triangular prism elements. 2D planar projections of the finite element meshes of the generic single and double loop models are shown in Fig. 6.

In vertical GHE applications, since the heat transfer is predominantly in the radial direction and the vertical heat flow in the system is insignificant, it is a reasonable approach to distribute the swept mesh on the vertical axis with refinements only close to layer interfaces, or the depths where the extrusion of the 2D geometry was stopped. This procedure leaves coarser vertical mesh inside the soil layers. There may be exceptions to this approach in certain cases, such that, the first several meters below the ground surface should

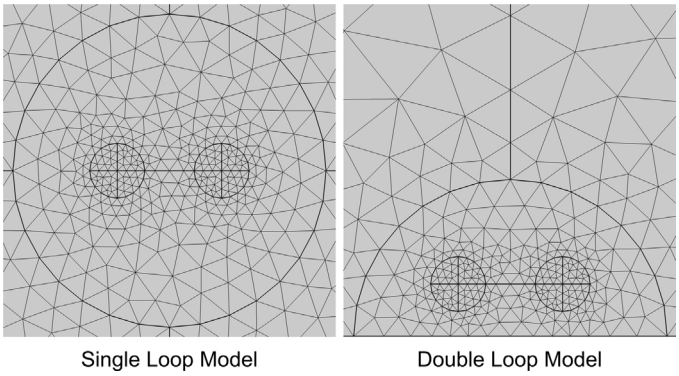


**Fig. 6.** 2D finite element meshes of the generic single and double loop models.

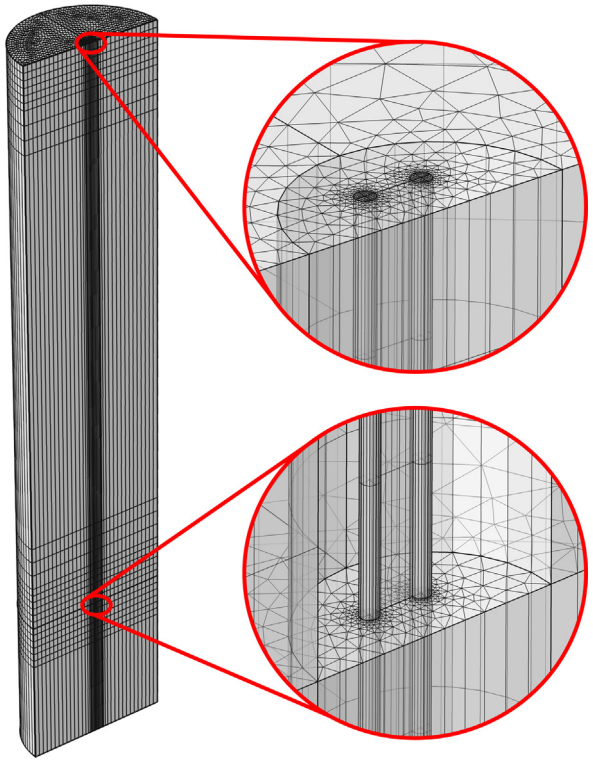

**Fig. 7.** Finite element mesh of a double loop energy pile model.

also be refined if the vertical temperature gradient caused by climatic effects will be considered in the model. The overall finite element mesh of a generic energy pile model with double loop configuration is shown in Fig. 7.

## 6. Physics of the thermal processes and model boundary conditions

The physics of the utilized problems in the proposed numerical model in order to simulate the operation of a GHE system can be divided into two categories: (1) the time dependent heat transfer problem in the volumetric domains, which is solved by calculating the temperature in each finite element mesh node; (2) the transient fluid flow and forced convection problems in the pipes, solved by evaluating the temperatures of the fluid and the pipe wall along the pipe axis.

In the solid domains such as pseudo pipes, grout, and soil, pure conductive heat transfer is anticipated which is governed by the

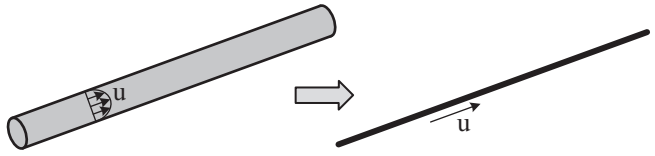


**Fig. 8.** Linear pipe elements reduce the 3D flow problem to 1D (after COMSOL, 2012).

following equation assuming that there is no internal heat generation:

$$\rho c_p \frac{\partial T}{\partial t} + \nabla \cdot (-\mathbf{k}\nabla T) = 0 \tag{11}$$

Eq. (11) is solved for temperature, $T$, making use of the assigned boundary conditions and the temperature coupling with the linear pipe elements. Boundary conditions designate the behavior of the numerical model during runtime and are used to build the sparse matrix solved thereafter for estimating the temperature changes. Either no heat flux (insulation – Neumann), or prescribed temperature (Dirichlet) boundary condition should be specified for the lateral and the bottom limits of the model. For the former case, it must be ensured that there is no temperature change at these boundaries while for the latter case; the heat flux on these boundaries must be zero throughout the runtime of the model. This can be achieved by setting the extent of the model at distances where heat exchange operations essentially have no effect. The Dirichlet boundary condition can only be used if the initial temperature of the ground is selected as a single value for all depths. For models with symmetrical geometry, no heat flux boundary condition is used on the symmetry plane.

The Neumann boundary condition with no heat flux can be expressed as:

$$q'' = (-\mathbf{k}\nabla T) = 0 \tag{12}$$

The fluid flow and heat transfer problem in the pipes are physically modeled using linear elements, reducing the 3D flow problem to 1D as shown in Fig. 8. Modeling pipes as curves in 2D or 3D provides great advantage in computational efficiency over meshing and computing 3D pipes with finite diameter.

The linear pipe element is an approximation of a heat exchanger pipe by modeling the internal fluid flow and the layered pipe wall; and solving the pipe flow and heat transfer problems simultaneously using built-in equations. The pipe flow problem is determined by solving the momentum and continuity equations given as (Barnard et al., 1966):

$$\rho_f \frac{\partial \mathbf{u}}{\partial t} = -\nabla p - f_D \frac{\rho_f}{2d_h}\mathbf{u}|\mathbf{u}| \tag{13}$$

and

$$\frac{\partial A_{pi}\rho_f}{\partial t} + \nabla \cdot (A_{pi}\rho_f \mathbf{u}) = 0 \tag{14}$$

The second term on the right-hand side in Eq. (13) represents the pressure drop due to viscous shear. The Darcy friction factor in Eq. (13) accounts for the continuous pressure drop along a pipe segment due to viscous shear, and is expressed as a function of the Reynolds number, Re and the ratio of the surface roughness to the hydraulic diameter, $e/d_h$.

$$f_D = f\left(Re, \frac{e}{d_h}\right) \tag{15}$$

The Darcy friction factor, $f_D$ can be estimated using the Churchill (1997) equation as follows:

$$f_D = 8\left[\left(\frac{8}{Re}\right)^{12} + (C_A + C_B)^{-1.5}\right]^{1/12} \tag{16}$$

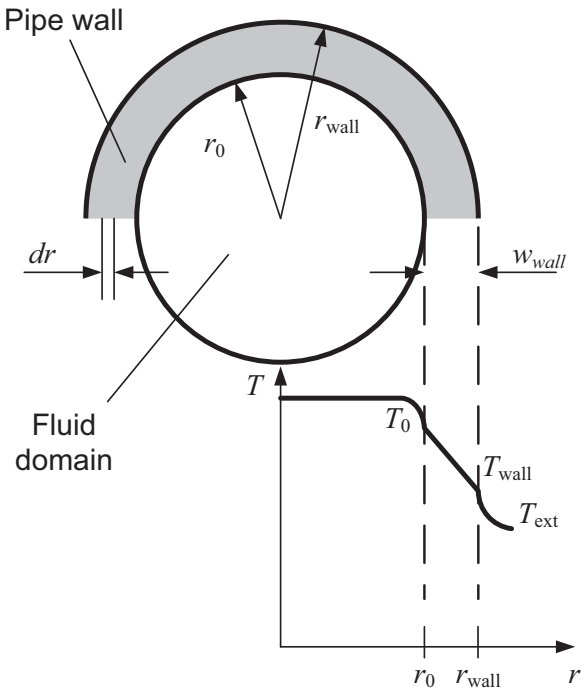


**Fig. 9.** Temperature distribution across the pipe wall (after COMSOL, 2012).

where $C_A$ and $C_B$ are factors given as:

$$C_A = \left[-2.457 \ln\left(\left(\frac{7}{Re}\right)^{0.9} + 0.27\left(e/d_h\right)\right)\right]^{16}$$

$$\text{and } C_B = \left(\frac{37530}{Re}\right)^{16} \tag{17}$$

Eq. (16) is valid for all flow conditions, i.e. laminar or turbulent. Moreover, $e$ in Eq. (17) denotes the absolute surface roughness of the pipe; and for plastic pipes, it is given as 0.0015 mm.

Reynolds number, Re is defined as the ratio of the inertial forces to the viscous forces, such that:

$$Re = \frac{\rho_f u d_h}{\mu} \tag{18}$$

Heat transfer in pipes problem is governed by the energy equation for an incompressible fluid flowing in a pipe:

$$\rho_f A_{pi} c_{pf} \frac{\partial T}{\partial t} + \rho_f A_{pi} c_{pf} \mathbf{u} \cdot \nabla T = \nabla \cdot A_{pi} k_f \nabla T + f_D \frac{\rho_f A_{pi}}{2d_h}|\mathbf{u}|^3 + q'_{wall} \tag{19}$$

The second term on the right hand side corresponds to friction heat dissipated due to viscous shear. The radial heat transfer from the surroundings into the pipe is given by:

$$q'_{wall} = (hZ)_{eff}(T_{ext} - T) \tag{20}$$

Fig. 9 shows the cross-section of the pipe-fluid domains and the temperature distribution across the pipe wall (COMSOL, 2012). With reference to this figure, the effective overall heat transfer coefficient per unit length of the pipe, including the internal film resistance and the wall resistance can be estimated as:

$$(hZ)_{eff} = \frac{2\pi}{\frac{2}{d_{pi}h_{int}} + \frac{\ln(d_{po}/d_{pi})}{k_p}} \tag{21}$$

The internal film resistance can be calculated using:

$$h_{\text{int}} = \text{Nu}\frac{k_f}{d_h} \tag{22}$$

Nusselt number is defined as the ratio of convective to conductive heat transfer across a boundary. For turbulent flow conditions, Nusselt number can be estimated using the correlation developed by Gnielinski (1976) as follows:

$$\text{Nu} = \frac{(f_D/8)(Re-1000)Pr}{1+12.7(f_D/8)^{1/2}(Pr^{2/3}-1)}, \quad \begin{matrix} 0.5 < Pr < 2000 \\ 3000 < Re < 6\times 10^6 \end{matrix} \tag{23}$$

In the numerical model, the external temperature outside of the pipes, $T_{\text{ext}}$ corresponds to the temperature field computed in the 3D domains. This provides automatic heat transfer coupling to the volumetric domains, considering the pipes as a line heat source. The coupling between the two physics nodes is accomplished through outer pipe wall temperature. However, there is a limitation in this approach. Since the pipes are made of linear elements, the outer pipe wall temperature is coupled to the temperature field of the volumetric domains located at the pipe axis. This introduces estimation errors, because the temperature field of the volumetric domains to be coupled should be located at a distance of pipe outside radius from the pipe axis. Another downside of this simplification is that, it does not account for the heat capacity of the pipes. A 'pseudo pipe' approach was developed as shown in Fig. 5 to overcome these issues. The diameter of these cylindrical solid domains is equal to the pipe outside diameter. The assigned material properties, which are presented in the next section, ensure the coupling of the temperature accurately, while accounting for the heat capacity of the pipes, as well.

## 7. Model validation

The proposed 3D numerical model is utilized to simulate two generic field thermal conductivity tests. Analysis results are compared with an analytical method. Philippe et al. (2009) recommend the use of infinite cylindrical source (ICS) model for small times. They showed that for a borehole radius of 5 cm, using ICS model for times less than 34 h limits the error level to 2%. In the present study, finite line source model is used for the validation of the proposed numerical model in order to capture the axial thermal effects occurring near the extremities of the heat exchanger. The influence of these end effects on the thermal response is significant for shorter GHEs, such as energy piles.

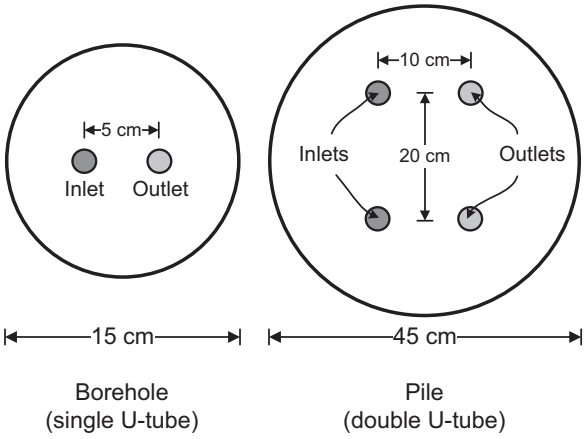


**Fig. 10.** Thermal conductivity test configurations for borehole and pile set-ups.

The thermal conductivity tests for the validation of the numerical model are selected as tests performed on a borehole with a single loop and an energy pile with double loop. The borehole is 15 cm in diameter and 100 m in length, whereas the energy pile is 45 cm in diameter and 20 m in length. The plan views of field test setups for each test, along with the loop placement and pipe leg spacing are given in Fig. 10.

The geothermal borehole is integrated with 3/4″ HDPE pipes and the energy pile with 1 1/4″ pipes, both with a standard dimension ratio (SDR) of 11. The geometrical parameters of the borehole and the energy pile are given in Table 1.

Two different material sets are used for modeling the pipes. Actual thermal conductivity of the HDPE pipe material ($0.39\,\text{W m}^{-1}\,\text{K}^{-1}$) is assigned to the line elements. These elements cannot have heat capacities since they are not volumetric elements.

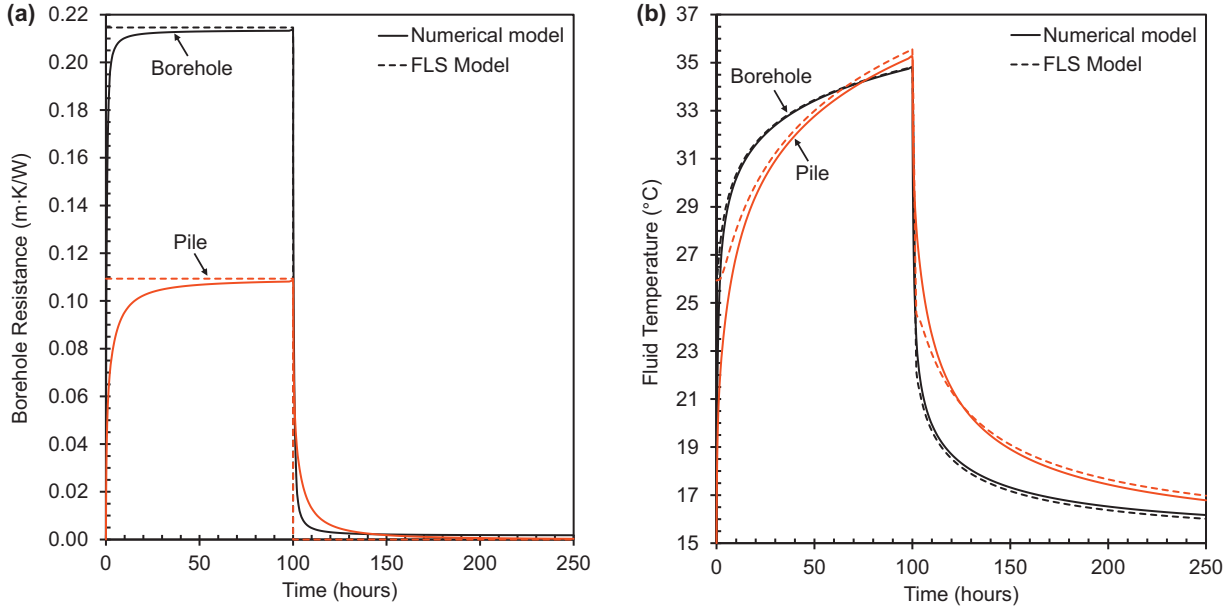


**Fig. 11.** Comparison between the proposed numerical model (solid line) and the analytical FLS model (dashed line): (a) thermal borehole and pile resistances during the analysis period, where steady state thermal resistances are calculated using line source approximation (Hellström, 1991); (b) mean fluid temperatures in the geothermal loops.

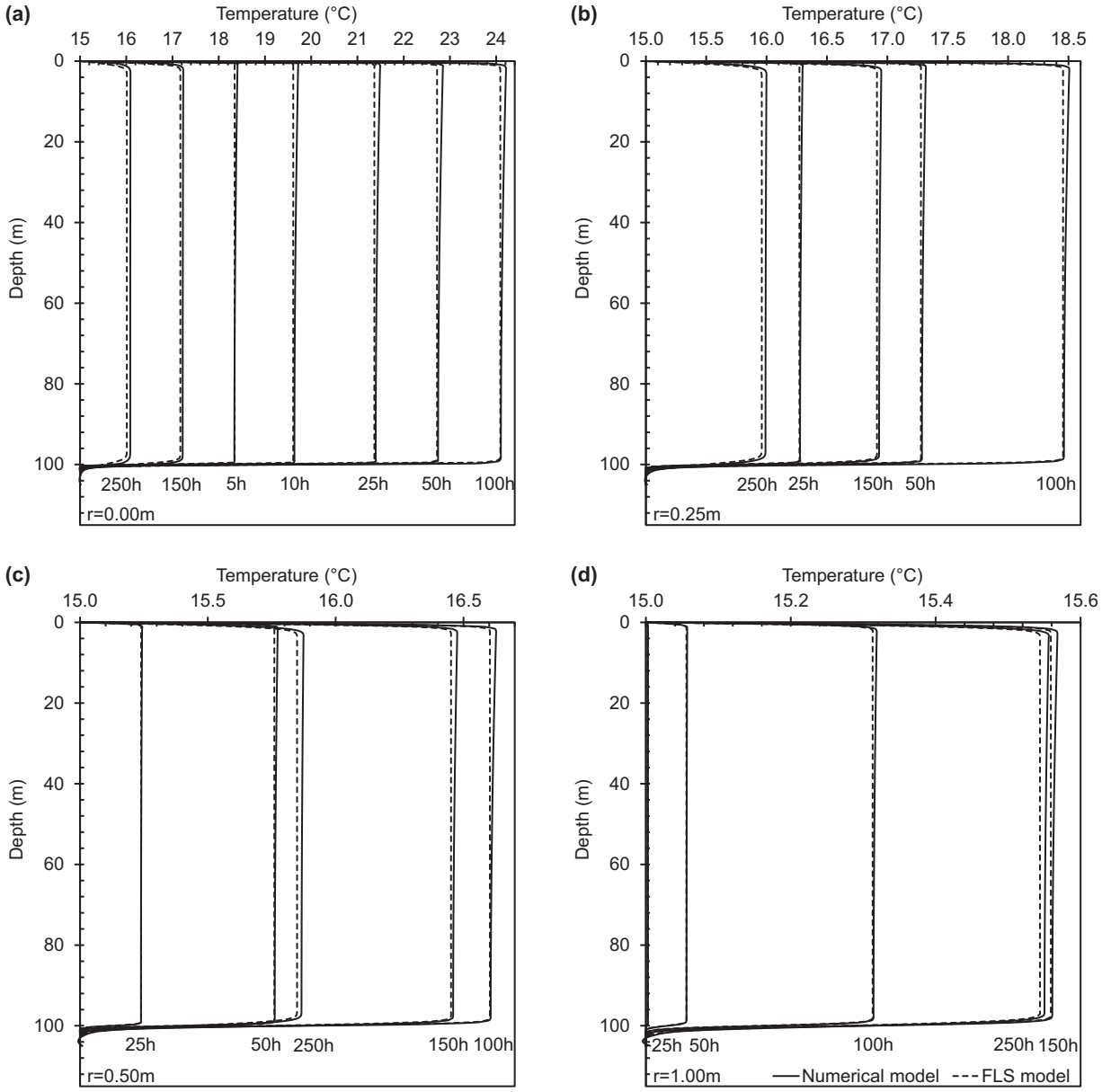


**Fig. 12.** Comparison between the temperature variations along the borehole depth estimated by the proposed numerical model (solid line) and the analytical FLS model (dashed line) at: (a) borehole wall; (b) 25 cm away from the borehole wall; (c) 50 cm away from the borehole wall; (d) 1 m away from the borehole wall.

**Table 1**
Dimensions of the borehole and the energy pile.

| Parameter | Borehole | Pile | Unit |
|---|---|---|---|
| Diameter | 150 | 450 | mm |
| Length | 100,000 | 20,000 | mm |
| Pipe inner diameter | 21.5 | 34.0 | mm |
| Pipe wall thickness | 2.4 | 3.8 | mm |
| Pipe shank spacing | 50 | 100 | mm |
| Loop spacing | – | 200 | mm |

To overcome this issue, the heat capacity of the pipes is assigned to the pseudo pipe elements surrounding these elements. The effective density of the pseudo pipe elements is estimated using the pipe volume ratio as a correction factor:

$$\rho_{p\,eff} = \rho_p \left( \frac{d_{po}^2 - d_{pi}^2}{d_{po}^2} \right) \quad (24)$$

Anisotropic thermal conductivity is assigned to the pseudo pipe elements and it is selected to be very high ($1000\,W\,m^{-1}\,K^{-1}$) in the horizontal plane and zero in the vertical direction to correct for the temperature coupling error.

The undisturbed ground temperature is selected to be 15 °C, which represents a moderate climate region. The thermal conductivity tests are performed by applying a constant heat rate of $50\,W\,m^{-1}$ for 100 h. The magnitude of the selected heat rate is within the range recommended by Kavanaugh et al. (2001). After loading, the temperatures are recorded for a recovery period of 150 h. Both for the numerical model and the finite line source model, the ground surface is kept at a constant temperature, which is equal to the undisturbed temperature. A mixture of water and propylene glycol with a concentration of 20% by volume is used as the heat exchange fluid. The thermal and rheological properties of the water–antifreeze solution are taken from the ASHRAE Handbook Fundamentals (ASHRAE, 2009). The thermal properties of the ground and the heat exchanger material are selected by referring to

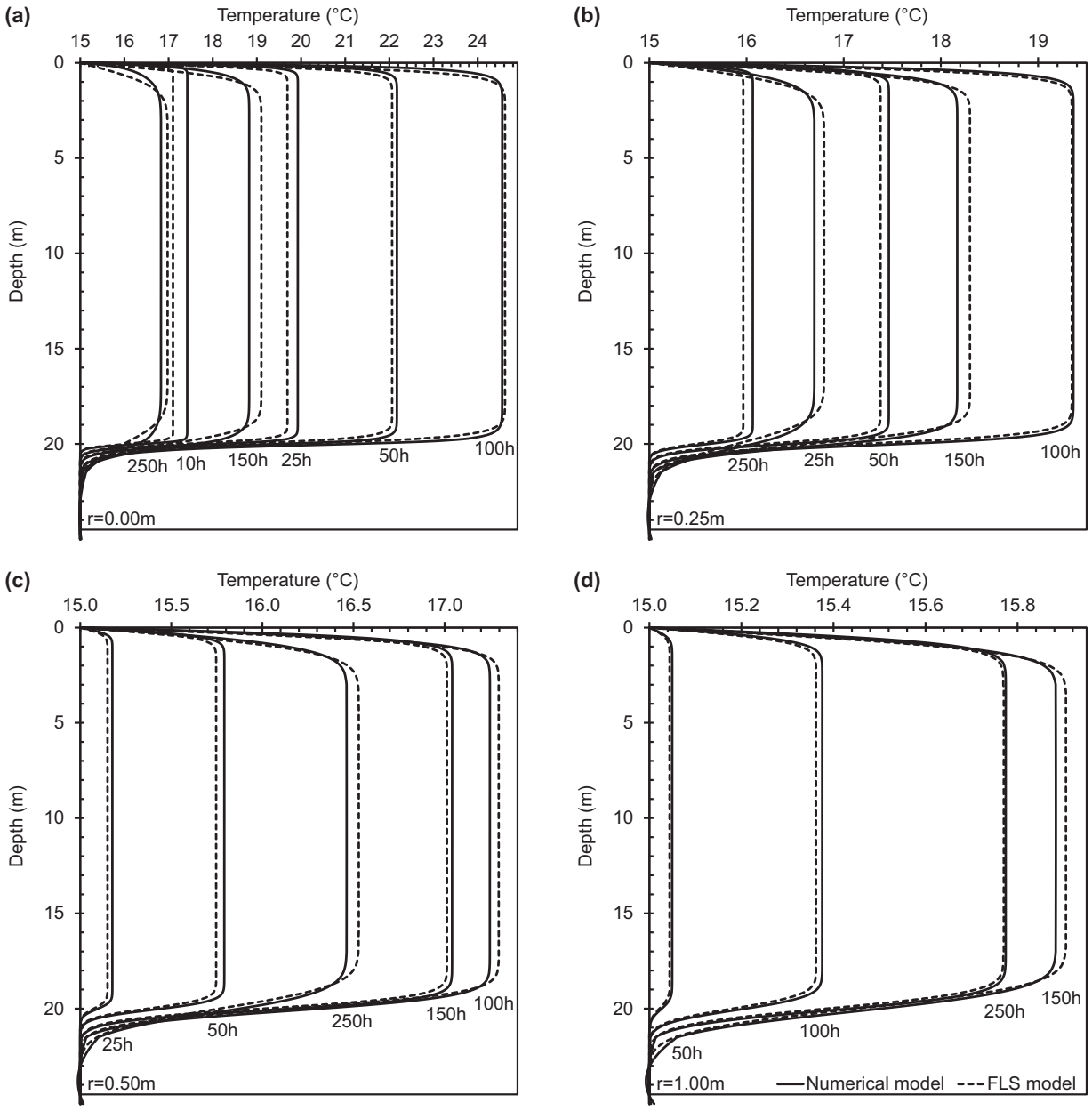


**Fig. 13.** Comparison between the temperature variations along the energy pile depth estimated by the proposed numerical model (solid line) and the analytical FLS model (dashed line) at: (a) pile wall; (b) 25 cm away from the pile wall; (c) 50 cm away from the pile wall; (d) 1 m away from the pile wall.

the studies by Farouki (1981) and Salomone et al. (1989). The input parameters used in the numerical analyses are listed in Table 2.

Two boundary conditions are defined on the inlet point of the linear pipe element: (1) volumetric flow rate, $\dot{V}$ ($m^3\,s^{-1}$); (2) prescribed temperature, $T_{in}(t)$ (K). The former is used to define the flow of circulation fluid inside the pipes, while the latter is used to define the heating of the fluid. Heat injection is accomplished by applying a temperature difference on the inlet boundary and it is expressed as:

$$T_{in}(t) = T_{out}(t) + \Delta T(t) \tag{25}$$

Applied temperature difference maintains a temperature difference between the inlet and the outlet throughout the heating period; simulating the heat injection into the system. $\Delta T(t)$ is a function of time, however; since the heat rate and the flow rate of the circulation fluid is selected constant, the temperature difference is constant during the heating period and it is zero during the recovery period. For the heating period, $\Delta T$ is estimated using:

$$q = \dot{V}\rho_f c_{pf}\Delta T$$
$$\Delta T = \frac{q}{\dot{V}\rho_f c_{pf}} \tag{26}$$

For optimizing the convergence of the model, a continuous step function is used as a multiplier while assigning the volumetric flow rate and the applied temperature difference, allowing a smooth transition from zero to the desired value in 0.1 s.

## 8. Results

The formulation in Eq. (5) is utilized for the analytical model and it is used to estimate the temperature variations along the depth of GHE at various time/radial distance combinations, starting from the borehole/pile wall. The steady state thermal resistance of the GHE

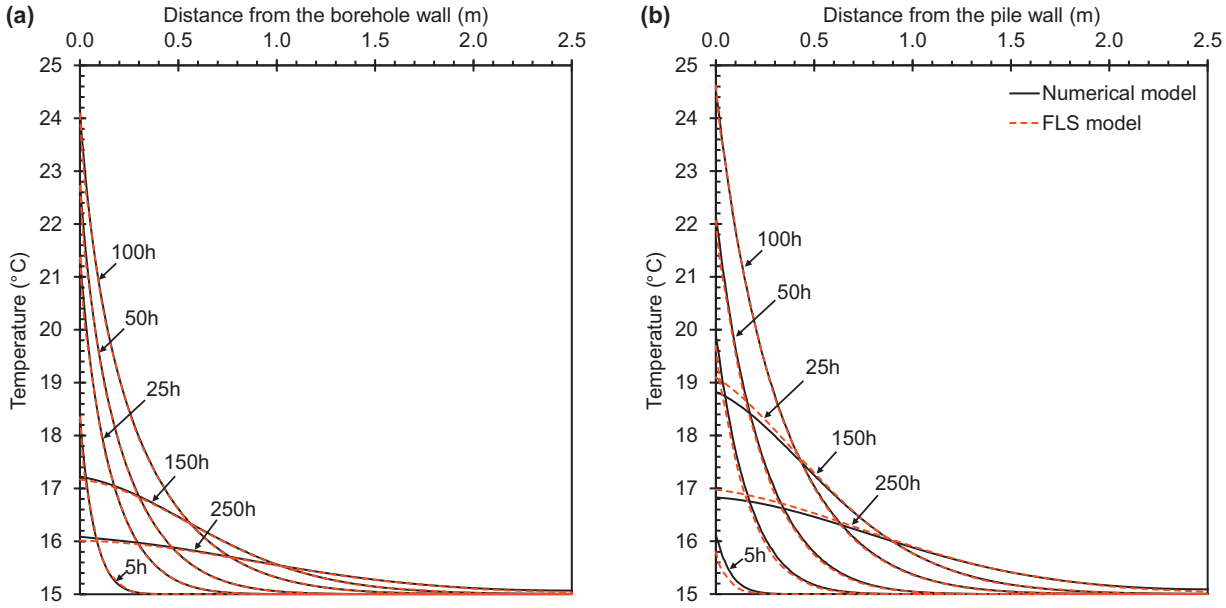


**Fig. 14.** Comparison between the temperature versus radial distance at mid-depth of GHE estimated by the proposed numerical model (solid line) and the analytical FLS model (dashed line): (a) borehole; (b) energy pile.

is calculated using Hellström's (1991) line source approximation as given by Eq. (10). The steady state thermal resistance has a constant value during the heating period and it is zero during the recovery period. The obtained average temperature of the GHE wall is then used to evaluate the mean fluid temperatures during the analysis period using Eq. (6).

On the other hand, GHE wall temperature in the numerical model is evaluated using a surface integration technique and overall thermal resistance of the GHE is calculated similarly as in the analytical method, using Eq. (6). The estimated thermal resistance is transient in nature, since mean fluid temperature and average wall temperature are time dependent. The comparison of the thermal resistances and the mean fluid temperatures estimated with both models are given in Fig. 11. Despite its smaller diameter, the thermal resistance of the borehole is almost twice of the energy pile. This is caused by the fact that the energy pile has a higher thermal conductivity and contains double U-tubes. It is also seen that both the analytical model and the numerical model result in similar fluid temperatures.

The temperature variations along the depth of the GHE are computed at the borehole/pile wall, and at radial distances of 25 cm, 50 cm and 1 m from the GHE wall. The temperature evaluations are performed for the analysis period with 5 h time steps. For the sake of simplicity, temperature profiles at 5 h, 10 h, 25 h, 50 h, 100 h, 150 h and 250 h are presented here. Moreover, for some distance/time

**Table 2**
Parameters used in the numerical analyses.

| Parameter | Value | Unit |
|---|---|---|
| Global parameters | | |
| Initial ground temperature | 15 | °C |
| Heat rate per depth (borehole) | 50 | W m$^{-1}$ |
| Heat rate per depth (pile) | 100 | W m$^{-1}$ |
| Circulation fluid | | |
| Flow rate | 20 | dm$^3$ min$^{-1}$ |
| Dynamic viscosity | 2.02 | mPa s |
| Thermal conductivity | 0.48 | W m$^{-1}$ K$^{-1}$ |
| Specific heat capacity | 3962 | J kg$^{-1}$ K$^{-1}$ |
| Density | 1020.91 | kg m$^{-3}$ |
| Linear pipes | | |
| Thermal conductivity | 0.39 | W m$^{-1}$ K$^{-1}$ |
| Pseudo pipes | | |
| Thermal conductivity | {1000, 1000, 0} | W m$^{-1}$ K$^{-1}$ |
| Specific heat capacity | 2300 | J kg$^{-1}$ K$^{-1}$ |
| Density (material) | 960 | kg m$^{-3}$ |
| Density (effective, 3/4″) | 319.28 | kg m$^{-3}$ |
| Density (effective, 1 1/2″) | 320.66 | kg m$^{-3}$ |
| Borehole (sand-bentonite) | | |
| Thermal conductivity | 1.00 | W m$^{-1}$ K$^{-1}$ |
| Specific heat capacity | 1600 | J kg$^{-1}$ K$^{-1}$ |
| Density | 1500 | kg m$^{-3}$ |
| Pile (reinforced concrete) | | |
| Thermal conductivity | 1.50 | W m$^{-1}$ K$^{-1}$ |
| Specific heat capacity | 1000 | J kg$^{-1}$ K$^{-1}$ |
| Density | 2500 | kg m$^{-3}$ |
| Ground | | |
| Thermal conductivity | 2.00 | W m$^{-1}$ K$^{-1}$ |
| Specific heat capacity | 1500 | J kg$^{-1}$ K$^{-1}$ |
| Density | 2000 | kg m$^{-3}$ |

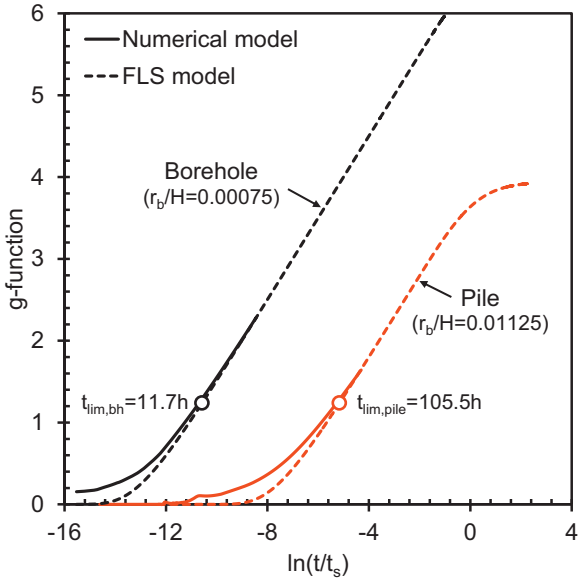


**Fig. 15.** Dimensionless g-functions for the borehole and the energy pile computed using the numerical model (solid line) and the analytical FLS model (dashed line).

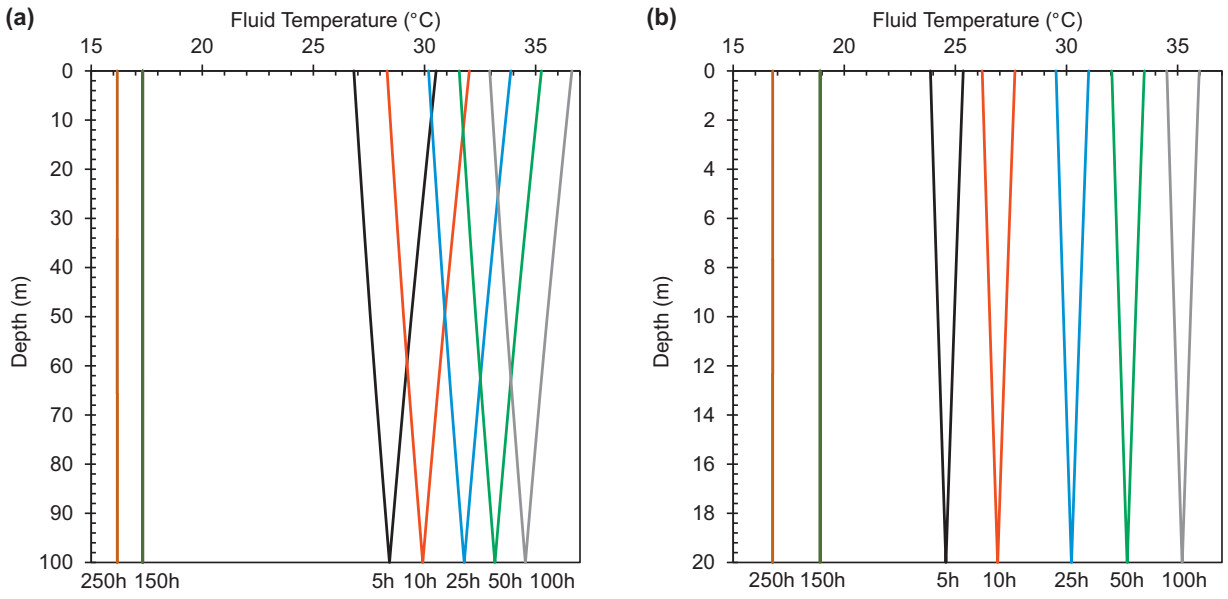


**Fig. 16.** Fluid temperature profiles along the depth of GHE estimated by the proposed numerical model: (a) borehole; (b) energy pile.

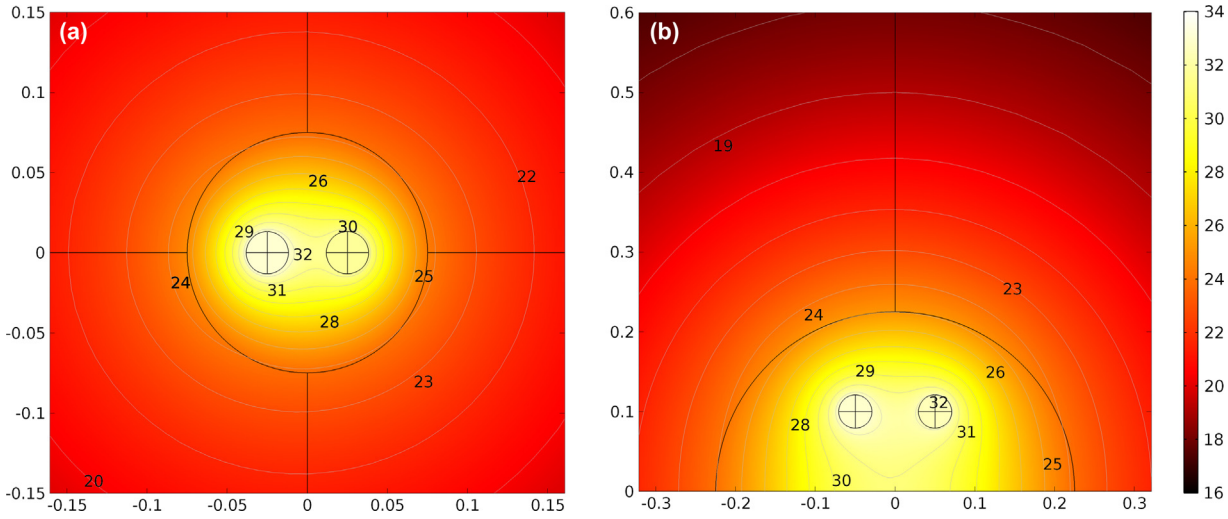


**Fig. 17.** Temperature contour plots within a cross-section at mid-depth of GHE at the end of heat injection period (at 100 h): (a) borehole; (b) energy pile.

combinations, temperature plots of various times are not shown on the figures, because they either overlap with each other or the temperature changes at these times are insignificant. The temperature profile plots at various times for the borehole and the energy pile are shown in Figs. 12 and 13, respectively.

It can be inferred that the temperature profiles calculated using analytical and numerical models for the borehole have slightly better agreement than the energy pile. This behavior is expected since the prediction of the finite line source model is more accurate in small diameter GHEs.

The temperatures at different times with respect to radial distance from the GHE wall are also evaluated at the mid-depth of the GHE. Fig. 14 shows the comparison plots between two models for the borehole and the energy pile at 5 h, 25 h, 50 h, 100 h, 150 h and 250 h. Similar to the temperature profiles, analytical and numerical results of temperature vs. radial distance for the borehole are slightly closer. Nevertheless, the numerical modeling approach proposed here results in very similar values with the analytical solution. The model serves as a useful tool to better understand the performance of GHE systems with different diameters and tube configurations.

Furthermore, the numerical results are used to develop g-functions for the simulated borehole and the energy pile (Fig. 15). The g-function model provides an efficient solution to simulate a single GHE or GHE fields with defined configurations over long timescales. The g-function is a normalized step response function that describes the temperature change at the GHE wall in response to a step heat input for a time step. It can be expressed as:

$$g\left(\frac{t}{t_s}, \frac{r_b}{H}\right) = \frac{2\pi k \cdot \Delta T_{bw}}{q'}, t_s = \frac{H^2}{9\alpha} \quad (27)$$

Eskilson (1987) developed hundreds of long-step g-functions for multiple borehole heat exchangers arranged in different configurations. In this approach, the thermal conductivities and capacities

of the materials inside the heat exchanger are neglected and as a result, the solution is only valid after a certain time, defined as:

$$t > \left(\frac{5r_b^2}{\alpha}\right) \quad (28)$$

Fig. 15 shows the comparison of g-functions of the borehole and the energy pile computed using the analytical and numerical models. In order to investigate a wider range, the analytical method results are extended to 20 years of heating in both cases. Using Eq. (28), the time limits indicating the validity of FLS model are computed as 11.7 h and 105.5 h for the borehole and the pile, respectively. It can be concluded that the g-functions computed with either model are in good agreement after the mentioned time limits in both cases.

Unlike the analytical solutions, the proposed numerical model allows estimating the fluid temperatures along the pipes and also the temperature distribution inside the GHE. The fluid temperature profiles for the borehole and the energy pile along the depth at 5 h, 25 h, 50 h, 100 h, 150 h and 250 h are presented in Fig. 16. Temperature contour plots within a cross-section at mid-depth of GHE at the end of heat injection period (at 100 h) are shown in Fig. 17.

## 9. Conclusions

In this study, a three dimensional numerical model for vertical GHE simulation is developed using a commercially available finite element simulation environment, COMSOL Multiphysics™ (COMSOL, 2012). The proposed numerical model uses a combination of 1D and 3D physics, such that, the flow and heat transfer inside the pipes are simulated using 1D elements and heat transfer in the grout and soil/rock mediums is represented in a 3D geometry. These two different modes are then fully coupled using the temperature field on the pipe exterior surface. This simplification introduces a coupling error, which is resolved by developing a 'pseudo pipe' approach. A similar technique which was previously used in a study by Marcotte and Pasquier (2008) is selected to optimize the finite element mesh of the model in order to reduce the number of elements. These approaches and the mesh generation technique are carefully studied in order to estimate the 3D transient heat and mass transport processes in the borehole/energy pile with satisfactory accuracy while keeping the computational effort minimum. A complete description of building steps of the model is also provided.

The validation of the proposed model is carried out by simulating two generic cases and comparing the numerical results with the results obtained from the finite line source model. A review of the theory of finite line source model (Ingersoll and Plass, 1948; Zeng et al., 2002) is also presented, along with modifications for variable heat rate (Yang et al., 2009). Moreover, a method developed by Hellström (1991) and presented by Zeng et al. (2003) is utilized to estimate the steady state thermal resistances in the borehole/energy pile in order to calculate the fluid temperatures analytically. Both models are used to simulate two generic cases, a borehole with a single U-tube and an energy pile with double U-tubes, respectively. In each case, a constant heating period of 100 h followed by a recovery period of 150 h, during which heating was stopped, is simulated.

The analysis results of the numerical and analytical models are compared by the average fluid temperatures, temperature profiles at several radial distance-time combinations, and temperature versus radial distance at mid-depth of the GHE at various times. The numerical model is verified and the results suggest that it can successfully simulate the operation of vertical geothermal heat exchangers. The numerical model proposed here is being implemented for analyzing several field thermal conductivity tests performed on energy piles with different sizes and loop configurations.

## Acknowledgements

The authors would like to express their gratitude for the support by the National Science Foundation under Grants No. 0928807 and 1100752. The first author is funded as a visiting scholar by the Turkish Council on Higher Education and Istanbul Technical University. These supports are greatly appreciated.

## References

Al-Khoury, R., Bonnier, P.G., Brinkgreve, R.B.J., 2005. Efficient finite element formulation for geothermal heating systems, part I: steady state. International Journal for Numerical Methods in Engineering 63, 988–1013.
Al-Khoury, R., Brinkgreve, R.B.J., 2006. Efficient finite element formulation for geothermal heating systems, part II: transient. International Journal for Numerical Methods in Engineering 67, 725–745.
American Society of Heating, Refrigerating and Air-Conditioning Engineers (ASHRAE), 2009. ASHRAE Handbook of Fundamentals. American Society of Heating, Refrigerating and Air-conditioning Engineers.
Austin III, W.A., (MSc Thesis) 1998. Development of an In-Situ System for Measuring Ground Thermal Properties. Oklahoma State University, Stillwater, OK, pp. 177.
Bandos, T.V., Montero, A., Fernandez de Cordoba, P., Urchueguia, J.F., 2011. Improving parameter estimates obtained from thermal response tests: effect of ambient air temperature variations. Geothermics 40, 136–143.
Barnard, A.C.L., Hunt, W.A., Timlake, W.P., Varley, E., 1966. A theory of fluid flow in compliant tubes. Biophysical Journal 6, 717–724.
Bauer, D., Heidemann, W., Diersch, H.-J.G., 2011. Transient 3D analysis of borehole heat exchanger modeling. Geothermics 40, 250–260.
Bennet, J., Claesson, J., Hellström, G., 1987. Multipole Method to Compute the Conductive Heat Fows to and Between Pipes in a Composite Cylinder. Notes on Heat Transfer. Department of Building Technology and Mathematical Physics, University of Lund, Lund, Sweden, pp. 42.
Bose, J.E., 1991. Design and Installations Standards. International Ground Source Heat Pump Association, Stillwater, OK.
Brandl, H., 2006. Energy foundations and other thermo-active ground structures. Geotechnique 56, 81–122.
Churchill, S.W., 1997. Friction factor equations spans all fluid-flow regimes. Chemical Engineering 84, 91–92.
Corradi, C., Schiavi, L., Rainieri, S., Pagliarini, G., 2008. Numerical simulation of the thermal response test within comsol multiphysics® environment. In: Proceedings of the COMSOL Conference, Hannover, p. 7.
COMSOL, 2012. COMSOL Multiphysics™ Version 4.3: User's Guide and Reference Manual. COMSOL Inc., Burlington, MA.
Energy Star, 2013. Overview of Geothermal Heat Pumps. Energy Star: A Joint Program of the U.S. Environmental Protection Agency and the U.S. Department of Energy. http://www.energystar.gov/index.cfm?c=geo_heat.pr_geo_heat_pumps
Eskilson, P., (PhD Thesis) 1987. Thermal Analyses of Heat Extraction Boreholes. Department of Mathematical Physics, Lund University, Lund, Sweden, pp. 264.
Farouki, O.T., 1981. Thermal Properties of Soils. United States Army Corps of Engineers Cold Regions Research and Engineering Laboratory, Hanover, NH, pp. 137.
Gnielinski, V., 1976. New equations for heat and mass transfer in turbulent pipe and channel flow. International Journal of Chemical Engineering 16, 359–368.
Gu, Y., O'Neal, D.L., 1998. Development of an equivalent diameter expression for vertical u-tubes used in ground-coupled heat pumps. ASHRAE Transactions 104, 347–355.
He, M., (PhD Thesis) 2012. Numerical Modelling of Geothermal Borehole Heat Exchanger Systems. De Montfort University, Leicester, UK, pp. 183.
Hellström, G., (PhD Thesis) 1991. Ground Heat Storage: Thermal Analyses of Duct Storage Systems. Department of Mathematical Physics, Lund University, Lund, Sweden.
Ingersoll, L.R., Plass, H.J., 1948. Theory of the ground pipe heat source for the heat pump. ASHVE Transactions 47, 339–348.
Kavanaugh, S.P., Xie, L., Martin, C., ASHRAE1118-TRP 2001. Investigation of methods for determining soil and rock formation from short term field tests. American Society of Heating, Refrigerating and Air-Conditioning Engineers, Inc., pp. 77.
Lamarche, L., Stanislaw, K., Beauchamp, B., 2010. A review of methods to evaluate borehole thermal resistances in geothermal heat-pump systems. Geothermics 39, 187–200.
Lund, J.W., Freeston, D.H., Boyd, T.L., 2011. Direct utilization of geothermal energy 2010 worldwide review. Geothermics 40, 159–180.
Marcotte, D., Pasquier, P., 2008. On the estimation of thermal resistance in borehole thermal conductivity test. Renewable Energy 33, 2407–2415.
Omer, A.M., 2008. Ground-source heat pumps systems and applications. Renewable & Sustainable Energy Reviews 12, 344–371.

Paul, N.D., (MSc Thesis) 1996. The Effect of Grout Thermal Conductivity on Vertical Geothermal Heat Exchanger Design and Performance. Mechanical Engineering Department, South Dakota State University, Brookings, SD, pp. 538.

Philippe, M., Bernier, M., Marchio, D., 2009. Validity ranges of three analytical solutions to heat transfer in the vicinity of single boreholes. Geothermics 38, 407–413.

Salomone, L.A., James, I.M., Bose, J.E., 1989. Soil and Rock Classification for the Design of ground-Coupled Heat Pump Systems: Field Manual. International Ground Source Heat Pump Association, Stillwater, OK, pp. 55.

Sanner, B., Karytsas, C., Mendrinos, D., Rybach, L., 2003. Current status of ground source heat pumps and underground thermal energy storage in Europe. Geothermics 32, 579–588.

Signorelli, S., Bassetti, S., Pahud, D., Kohl, T., 2007. Numerical evaluation of thermal response tests. Geothermics 36, 141–166.

Thomson, W. (Lord Kelvin), 1884. Mathematical and Physical Papers, vol. 2. Cambridge University Press, London, UK, pp. 41–60.

Yang, W., Shi, M., Chen, Z., 2009. A variable heat flux line source model for boreholes in ground coupled heat pump. In: Proceedings of Asia-Pacific Power and Energy Engineering Conference (APPEEC 2009), Wuhan, China, March 28–31, p. 4.

Yavuzturk, C., (PhD Thesis) 1999. Modeling of Vertical Ground Loop Heat Exchangers for Ground Source Heat Pump Systems. Oklahoma State University, Stillwater, OK, pp. 231.

Yavuzturk, C., Spitler, J.D., 1999. A short time step response factor model for vertical ground loop heat exchangers. ASHRAE Transactions 105, 475–485.

Yu, M.Z., Diao, N.R., Su, D.C., Fang, Z.H., 2002. A pilot project of the closed-loop ground-source heat pump system in China. In: Proceedings of IEA 7th Heat Pump Conference, Beijing, China, May 19–22, pp. 356–364.

Zanchini, E., Lazzari, S., Priarone, A., 2010a. Effects of flow direction and thermal short-circuiting on the performance of small coaxial ground heat exchangers. Renewable Energy 35, 1255–1265.

Zanchini, E., Lazzari, S., Priarone, A., 2010b. Improving the thermal performance of coaxial borehole heat exchangers. Energy 35, 657–666.

Zeng, H.Y., Diao, N.R., Fang, Z.H., 2002. A finite line-source model for boreholes in geothermal heat exchangers. Heat Transfer—Asian Research 31, 558–567.

Zeng, H., Diao, N., Fang, Z., 2003. Heat transfer analysis of boreholes in vertical ground heat exchangers. International Journal of Heat and Mass Transfer 46, 4467–4481.